

**Weierstraß-Institut**  
**für Angewandte Analysis und Stochastik**  
**Leibniz-Institut im Forschungsverbund Berlin e. V.**

Preprint

ISSN 0946 – 8633

**Multiscale modeling of palisade formation in  
glioblastoma multiforme**

Alfonso Caiazzo<sup>1</sup>, Ignacio Ramis-Conde<sup>2</sup>

submitted: Sep 23, 2014

<sup>1</sup> Weierstrass Institute  
Mohrenstr. 39  
10117 Berlin  
Germany  
E-Mail: Alfonso.Caiazzo@wias-berlin.de

<sup>2</sup> Universidad de Castilla la Mancha (UCLM)  
Facultad de Educación de Cuenca  
Spain  
E-Mail: ignacio.ramis@uclm.es

No. 2012  
Berlin 2014



---

2010 *Mathematics Subject Classification.* 65P99, 92-08, 92B05.

*Key words and phrases.* Palisades, glioblastoma, multiscale hybrid modeling, force-based, finite elements.

Edited by  
Weierstraß-Institut für Angewandte Analysis und Stochastik (WIAS)  
Leibniz-Institut im Forschungsverbund Berlin e. V.  
Mohrenstraße 39  
10117 Berlin  
Germany

Fax: +49 30 20372-303  
E-Mail: [preprint@wias-berlin.de](mailto:preprint@wias-berlin.de)  
World Wide Web: <http://www.wias-berlin.de/>

## Abstract

Palisades are characteristic tissue aberrations that arise in glioblastomas. Observation of palisades is considered as a clinical indicator of the transition from a noninvasive to an invasive tumour. In this article we propose a computational model to study the influence of genotypic and phenotypic heterogeneity in palisade formation. For this we produced three dimensional realistic simulations, based on a multiscale hybrid model, coupling the evolution of tumour cells and the oxygen diffusion in tissue, that depict the shape of palisades during its formation. Our results can be summarized as the following: (1) we show that cell heterogeneity is a crucial factor in palisade formation and tumour growth; (2) we present results that can explain the observed fact that recursive tumours are more malignant than primary tumours; and (3) the presented simulations can provide to clinicians and biologists for a better understanding of palisades 3D structure as well as glioblastomas growth dynamics.

## 1 Introduction

Glioblastoma multiforme is the most aggressive and malignant type among all brain tumours, with a mean survival rate of 17 weeks without treatment and between 30 and 37 weeks for treated patients, depending on treatment. In addition, long term survival probability to glioblastoma is considered to be less than 3% [11]. Glioblastomas can arise as a new tumour and quickly grow, invading the brain tissue (novo glioblastoma); or they can develop from low grade astrocytomas (type I and II) as a recursive tumour (secondary) [11]. The principal histologic features of glioblastoma are the presence of necrotic regions; the vascularization of the tumour and the highly invasiveness of the malignant cells. This last characteristic is what ultimately makes glioblastoma lethal, as surgical removal of the tumour is not enough to eliminate all the malignant cells.

For arising as a secondary tumour, genotypic and phenotypic transitions of the malignant cells are crucial events [28]. While in lower grade gliomas cells are replicative and the tumour profile is confined into a determinate region; in glioblastomas the malignant cells spread out and invade the nearby parenchyma [10, 1]. To acquire the invasive abilities, malignant cells undergo a series of changes allowing the switch from aerobic to anaerobic metabolism. Once the tumour has grown up

to the state of creating hypoxic regions the cells enhance the Warburg effect when undergoing anaerobic metabolism [1, 5]. As a consequence they secrete lactate acid into the extracellular medium modifying the PH. The lack of oxygen and the increase of acidity of the environment may work as a natural selective process. Those cancer cells that do not have the capabilities to resist high lactate concentrations and longtime anaerobic metabolism may die. The result is a tumour where the malignant cells have increased their invasive capabilities as well as anoxia resistance [5, 13]. In addition the PH change plays counter healthy cells that are not as well adapted to acid environments as malignant cells.

The next step in the invasive cascade is enhancing the migrating mechanisms. Intracellular pathways such as the adhesive and enzymatic machinery are activated in order to degrade and migrate throughout the nearby tissue [30, 27, 25]. In addition, a set of endocrine factors such as VEGF are released into the environment to stimulate the formation of vasculature to compensate the lack of oxygen and nutrients produced as a consequence of high spatial competition [35].

The result is an aberrant hypervascularized environment where the malignant cells have spread out breaking the initial non-invasive geometry of the tumour. In this scenario, removal of the tumour and examination of 2D dimensional cuts under microscopy allows to differentiate areas of rows of malignant cells forming structures that wide from a wall-like shape to ellipsoidal rings. This process, in reference to the geometrical similarity that reminds ancient wood fortresses, is known as palisade formation.

## **1.1 Palisade formation**

How do palisades arise is still an open debate, however there are two principal accepted hypotheses, which differ in their initial conditions but are characterized by very similar underlying mechanisms [2, 3].

The first hypothesis is based on the formation of necrotic regions as a consequence of high cell confluence. At certain spatial positions of the growing glioblastoma, high cellular confluence may occur due to intense replication. Competition for oxygen and/or other nutrients may result in a local phenotypic change. Those cells that do not have enough nutrients may develop an invasive phenotype that allows them to migrate to better irrigated areas. As a consequence, a collective migration process towards nearby vessels is enhanced, leading to the characteristic palisade shape.

The second hypothesis considers palisade formation as a result of vessel collapse. Since palisades can be localized around occluded vascular vessels in glioblastomas [2, 3], this aspects suggests the following formation process. Initially the tumour grows around a vessel. This position facilitates the tumour supply of oxy-

gen and nutrients. The cells that are closest positioned to the vessel obtain easier nutrients and oxygen than those positioned at the outer part of the tumour [8]. At certain moment the tumour grows up to the size of exerting a pressure that results in vessel collapse. This moment represents a dramatical change for those cells that were positioned nearby to the vessel, which lack oxygen and nutrient supply as they are now at the centre of the tumour. As a consequence they become hypoxic and, if the tumour geometry or the irrigating vasculature do not change, they die of anoxia. At the outer rim of the tumour, the effects of vessel collapse are different. At this position the cells are not immersed in the tumour mass and when lack of oxygen and nutrients occurs they can activate migration mechanisms that allow them to invade the nearby tissue in the search for areas where oxygen and nutrients are available. The collective migration of these cells results in the formation of a palisade [1, 2, 3, 21].

## **1.2 Importance of cellular genotypes heterogeneity**

Despite the fact that often literature characterizes palisades solely as zones of high cellular confluence, there are two other important factors inseparable to palisade formation. Firstly, conjoined to palisade formation the tumour front acquires an invasive profile. And, secondly, the invaded healthy tissue at certain distance from the palisade is colonized by malignant cells expressing normoxic and hypoxic phenotypes [5, 9].

The colonizing process depends strongly on the particular characteristics of each cell composing the invasive front. The sensitivity of each cell to oxygen conditions determines the switch from normoxic to hypoxic phenotype. This sensitivity is regulated by the particular cellular genotype that governs the activation of genes that switch to anaerobic metabolism and enhance invasion mechanisms. Thus it is essential to understand how the particular phenotypic response of each cell depends on the cellular genotype.

Many theoretical models consider that two cells with identical genotype express the same phenotype under identical environmental conditions. However cellular individual response is likely to differ among cells, despite they have identical genotype or not [32, 6, 34, 23, 33, 18, 29]. The cellular genotype does not determine cell behavior in a deterministic fashion but it rather works as an inherited starting profile stochastically sensitive to both external and endocrine influences [6, 19, 15].

In this article we investigate the importance of genotypic heterogeneity within the tumour cells population using a realistic mathematical model. Recently, Perez-Garcia and Martinez-Gonzalez [21, 24, 22] and Geerle and Neelander [14] approached this question via continuous (one-dimensional and two-dimensional) models of palisade formation and tumour growth based on coupled reaction-diffusion

equations. Inspired by these works, we create a three-dimensional multiscale hybrid model, which combines a particle individual forced-based model for the tumour growth, taking into account the principal biophysical properties of the cells, and a continuum approach for simulating the oxygen diffusion into the tissue, which drives the phenotype switching within the cell population. In particular, the reaction–diffusion equation for the oxygen is solved via a finite element method on a tetrahedral mesh, handling the presence of blood vessel within the tissue using an immersed boundary method [7]. This approach does not require the discretization of vessel geometries within the finite element mesh, allowing to simulate an arbitrary three-dimensional vascularization. Furthermore, we compare two different simulation scenarios that represent a *deterministic genotypes* model and a *stochastic genotypes* model. In the deterministic scenario two cells with the same genotypic profile react identically under the same environmental conditions. In contrast, in the stochastic scenario, two cells with identical genotype may behave differently under identical oxygen conditions.

The paper is organized as follows. The multiscale model is presented in Section 2, describing in details the individual model for cells (Section 2.1), the finite element approach for the oxygen (Section 2.2) and the multiscale coupling conditions (Section 2.3). The numerical results are presented in Section 3, analyzing in particular the cases of deterministic (Section 3.1) and stochastic (Section 3.2) genotype models. Finally, the conclusions are drawn in Section 4.

## 2 The multiscale hybrid model

Glioblastoma growth and invasion are complex multiscale and multiphysics processes. On the one hand, the growth of the tumour can be described by the dynamics of a cell population undergoing phenotypic changes, which strongly depends on the availability of nutrients (e.g., oxygen) in the environment, provided by the surrounding vasculature. On the other hand, oxygen diffusion in the healthy and tumour tissue depends on the tumour configuration, and in particular on the nutrient consumption rates of the tumour cells.

These two processes (cell dynamics and oxygen diffusion) evolve on very different temporal and spatial scales. The characteristic temporal mesoscale of the cells colony biology is of the order of minutes (considering a cell cycle of about 16h), while the transient dynamics of the oxygen, i.e. the time needed for the oxygen concentration to reach an equilibrium stage according to environmental changes, happens on a faster time scale (order of seconds). At the same time, the cellular spatial scale (assuming cell diameters of  $O(\mu\text{m})$ ) is much smaller than the characteristic spatial scale of the distribution of oxygen concentration, which is assumed

to vary smoothly within the tissue. These considerations allow to represent the coupled multiscale system in the *scale-separation map* (see, e.g., [4]) drawn in Figure 1.

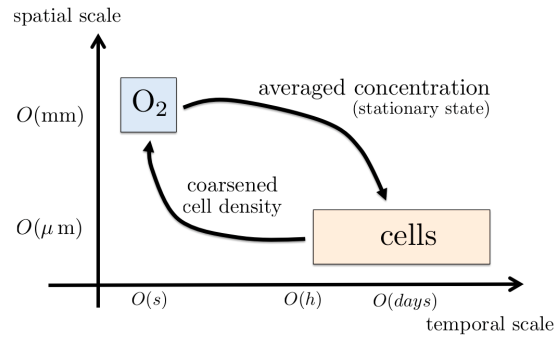


Figure 1: The scale separation map for the multiscale cells–oxygen model. The cells evolve on a spatial scale  $O(\mu\text{m})$ , smaller than the one of the oxygen diffusion in the tissue ( $O(\text{mm})$ ), but on a much slower time scale ( $O(\text{h})$  versus  $O(\text{s})$ ). The two subproblems are coupled across these scales through a coarsening of the cell distribution in space and by using the stationary approximation for the oxygen diffusion.

Our computational approach to model glioblastoma is based on the idea of *Complex Automata* (CxA) (see, e.g., [4, 17, 31]), in which a multiscale process is described in terms of *single scale models* interacting across the scales through appropriate multiscale coupling conditions. In particular, we consider two single scale models (see Figure 1), an *individual based* model for the cells (described in detail in Section 2.1), considered as viscoelastic spheres interacting with each other through mechanical forces and cell-cell signaling, and with the surrounding tissue, and a *finite element* model for the oxygen diffusion into the healthy and tumour tissues (Section 2.2). These single scale models are coupled as follows. The oxygen depends on the cells through the spatial cell distribution, which is obtained upscaling of the cell population up to the spatial resolution of the finite element mesh. On the other hand, the concentration of nutrients available to each cell is obtained evaluating at the center of the cell the steady-state oxygen concentration. More details on the coupling interfaces are given in Section 2.3.

## 2.1 Modelling the cells

The cells are modeled using an individual based approach, described by the following variables:

- cell center position  $\mathbf{x}$ ;

- cell radius  $r$ ;
- oxygen status  $\sigma$ ;
- position in the cell cycle.

Each cell is considered as a visco-elastic sphere that grows, divides, acquires phenotypic profiles and interacts with other cells.

### 2.1.1 Cell-cell interactions

Astrocytes shape can vary depending on the environment and on the degree of differentiation, but they are generally characterized by a central quasi-spherical part and a set of extended processes. To model the tumour cells we neglect the processes and consider the central part as a viscoelastic sphere undergoing small deformations. The adhesive-repulsive forces between cells are modelled by a modified Hertz model [27] described below.

Denoting by  $\mathbf{x}_i$  the position of the  $i$ -th cell and neglecting inertia terms as in [27] the cell movement is governed by the following ordinary differential equation:

$$\underbrace{\Gamma \dot{\mathbf{x}}_i(t)}_{\text{friction}} + \underbrace{f_i(t)}_{\text{noise}} = \underbrace{\sum_{j=1}^{N_{\text{cells}}(t)} \mathbf{F}_{i,j}(t)}_{\text{cell-cell forces}}, \quad (1)$$

where  $\dot{\mathbf{x}}_i$  is the cells velocity;  $\Gamma$  is a 3-dimensional tensor that models the physical structure of the environment, for simplicity assumed to be diagonal, i.e.,  $\Gamma_{l,k} = \gamma \delta_{l,k}$ ;  $f_i$  is a normal noise function that accounts for the fluctuation of the cells within the tissue;  $N_{\text{cells}}(t)$  is the total number of cells at time  $t$ . Finally,  $\mathbf{F}_{i,j}(t)$  is the attractive-repulsive forces exerted by the neighbour cell  $j$ , given by

$$\mathbf{F}_{i,j} = \underbrace{\frac{2}{3} \left( \frac{E}{1-\nu^2} \right) r_{ij}^{\frac{3}{2}} \sqrt{\frac{r_i r_j}{r_i + r_j}}}_{\text{repulsion}} - \underbrace{\alpha r_{ij} \left( r_i - \frac{r_{ij}}{4} \right)}_{\text{adhesion}}, \quad (2)$$

where  $r_i$  and  $r_j$  denote the radii of cell  $i$  and  $j$ , respectively,  $r_{ij}$  stands for the mutual distance between them,  $E$  and  $\nu$  denote the Young moduli and Poisson number, respectively, and  $\alpha$  is the adhesion coefficient depending on surface bonds.

Denoting with  $\Delta t_{\text{cells}}$ , equation (1) is solved explicitly at each time iteration for each cell, yielding

$$\mathbf{x}_i(t^{n+1}) = \mathbf{x}_i(t^n) + \frac{\Delta t_{\text{cells}}}{\gamma} \left( -f_i(t^{n+1}) + \sum_{j=1}^{N_{\text{cells}}(t^n)} \mathbf{F}_{i,j}(t^n) \right) \quad (3)$$

### 2.1.2 Cell cycle

The cells expressing normoxic phenotype can multiply by cellular mitosis with a probability inverse to a cell cycle length of about 16 hours ( $1/T_{CC}$ ). After division, the daughter cells grow rapidly up to acquiring the cells mother size. However, cell division is not allowed if the compression of the cell by neighbors is too high. This is taken into account in the model by allowing mitosis only if the repulsive force of the modified Hertz model (2) is below a given threshold.

### 2.1.3 Cell phenotypes

Each cell is characterized by different phenotypic states, depending on the amount of oxygen available. As in [21, 24, 22], we distinguish between normoxic, hypoxic, or death. The transition from one state to another is controlled by the amount of oxygen available in the nearby environment. If the oxygen concentration at the cellular spatial location stays above a determinate threshold ( $\tau_{hypo}$ ) then the cell remains normoxic performing aerobic metabolism. If the oxygen concentration falls below  $\tau_{hypo}$ , the cell becomes hypoxic and stops consuming oxygen. The activation of anaerobic metabolism of hypoxic cells [30, 21, 26] is modelled by increasing by one order of magnitude the random movement term of equation 2 [21]. Hypoxic cells that address to gain spatial locations with oxygen levels over the hypoxia threshold ( $\tau_{hypo}$ ) may revert into a normoxic phenotype with a probability  $p = 1/24$  hours. Ultimately, if oxygen concentration decreases below a dramatic threshold ( $\tau_{dead}$ ), the cells undergo apoptosis by anoxia [21]. At this point, cells move only as a consequence of mechanical forces.

### 2.1.4 Genotype models

Furthermore, we consider two different models to study the cell genotypic behavior. In the *deterministic genotype model*, each cell that undergoes mitosis produces two daughters that behave identically under the same exact oxygen conditions, i.e. for which the phenotype transition is regulated by the same treshold. The diagram in Figure 2 (left) shows how oxygen concentration determines within the cell population the switch between normoxic and hypoxic phenotypes in the deterministic genotypes model.

In the *stochastic genotypes model*, after mitosis, the daughter cell acquires a different sensitivity to oxygen conditions than the progenitor. This is modelled by assigning to the daughter cell a hypoxia threshold different from the one of the progenitor, and taken from an uniform distribution  $on_i = U(\mu_i, \sigma)$  with mean  $\mu_i = 12$  and standard deviation  $\sigma = D^2/12$ , where the parameter  $D$  regulates the stochasticity of the system. The diagram in Figure 2 (right) shows how oxygen concentration de-

termines the switch to hypoxic phenotype within the *stochastics genotypes model*. The principal difference between this approach and a traditional model of genotype mutations is that we are considering the variation of behavior in each cell of the population. In contrast, if one considers genotypic mutations across lineage, the behavior of each genotypic family is similar or identical, and variations may appear only when mutations occur [26]. Thus our problem is substantially different and allows for a much faster variability in the evolutionary dynamics.

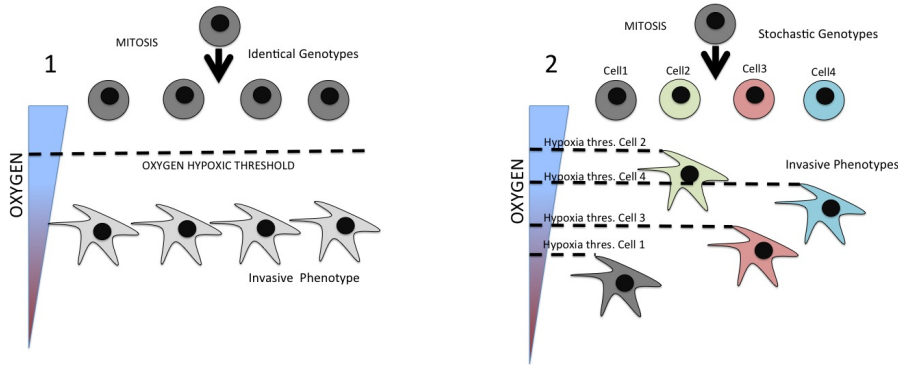


Figure 2: Diagram showing the two genotype scenarios. In the deterministic model (left), every time a cell replicates produces two daughters expressing the same behaviour as the progenitor. This profile determines uniquely via an oxygen threshold the switch between the normoxic and hypoxic phenotypes. In the stochastic model (right), after mitosis, the daughter cells can acquire a different respond than the progenitor despite of having the same genotype. This is modeled by providing each cell a different oxygen threshold under which the cell becomes hypoxic.

## 2.2 Diffusion-Reaction equation

The oxygen concentration in the tissue is modeled via a reaction-diffusion equation, containing source terms describing the oxygen flux from the blood vessels and sink terms representing the oxygen consumption of the cells.

Let us denote with  $\Omega$  the tissue domain and with  $c_{O_2}$  the oxygen concentration. We assume that oxygen diffuses within the cellular tissue homogeneously with a known diffusion constant  $D_{O_2}$ , and that each cell consumes oxygen at a given rate, equal to  $\mu_N$  or  $\mu_H$  for normoxic and hypoxic cells, respectively (dead cells do not consume any nutrient). Furthermore, we consider that the oxygen is constantly diffused into the domain at a rate  $\phi_v$  from a neighbor blood vessels (see Figure 3). Denoting the vessel domain by  $\Omega_v$ , the oxygen flux  $\phi_v$  through the boundary  $\partial\Omega_v$  is proportional to the concentration difference between the vessel and the tissue,

according to a filtration law:

$$\phi_v = \frac{1}{J_v}(c_v - c_{O_2}). \quad (4)$$

In (4),  $c_v$  denotes the oxygen concentration inside the vessel and  $J_v$  is the filtration coefficient.

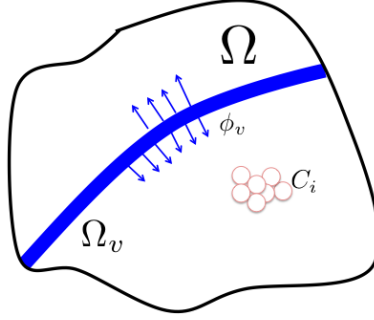


Figure 3: Sketch of the domain for the coupled model:  $\Omega$  denotes the oxygen concentration domain for the finite element model,  $\Omega_v$  denotes the blood vessel, and  $C$  denotes the space occupied by the cell population.

Let us denote with  $C_i(t)$  and  $\mu_i(t)$  the space occupied by the  $i$ -th cell and its consumption rate at time  $t$ , respectively. The oxygen concentration is governed by the following reaction-diffusion equation

$$\left\{ \begin{array}{l} \partial_t c - D_{O_2} \Delta c + \sum_{i=1}^{N_{\text{cells}}(t)} \chi_{C_i(t)} \mu_i(t) c = 0, \quad \text{in } \Omega \\ \frac{\partial c}{\partial n} = \phi_v = \frac{1}{J_v}(c_v - c), \quad \text{on } \partial\Omega_v \\ \frac{\partial c}{\partial n} = 0, \quad \text{on } \partial\Omega / \partial\Omega_v \end{array} \right. \quad (5)$$

where  $\chi_{C_i}$  stands for the characteristic function of the subdomain  $C_i$ , and the last equation imposes a free-flux boundary condition at the tissue external boundaries (i.e. the boundaries not belonging to any vessel wall).

Moreover, due to the time scale separation between the oxygen diffusion model and the cellular tissue growth, for the purposes of the coupled model we are only interested in the steady state oxygen concentration. Hence, given the cell distribution at a time  $t^{cells}$ , we only seek the stationary solution of equation (5), which describes the concentration field depending on the current cell configuration. Ne-

glecting the inertia term, problem (5) can be then rewritten as

$$\begin{cases} -D_{O_2}\Delta c + \left(\mu_N R_N^{cells}(t^{cells}) + \mu_H R_H^{cells}(t^{cells})\right) c = 0, & \text{in } \Omega \\ \frac{\partial c}{\partial n} = \phi_v = \frac{1}{J_v}(c_v - c), & \text{on } \partial\Omega_v \\ \frac{\partial c}{\partial n} = 0, & \text{on } \partial\Omega/\partial\Omega_v \end{cases} \quad (6)$$

where we have introduced the functions  $R_N^{cells}(t; \mathbf{x})$  and  $R_H^{cells}(t; \mathbf{x})$  denoting the space dependent densities of normoxic and hypoxic cells, respectively.

### 2.2.1 Finite element formulation

The time independent equation (6) is solved numerically using a finite element method. In order to describe the approach, let us introduce the standard Sobolev space  $V = H^1(\Omega)$  and denote with  $(\cdot, \cdot)_\Omega$  the standard  $L^2$  scalar product.

Testing (6)<sub>1</sub> by a function  $q \in V$  and integrating by parts, we obtain the following weak formulation of problem (6): Find  $c \in V$  such that

$$(D\nabla c, \nabla q)_\Omega + \sum_{\alpha=N,H} (\mu_\alpha R_\alpha^{cells}(t^{cells})c, q)_\Omega + \underbrace{\left(\frac{1}{J_v}(c - c_v), q\right)_{\partial\Omega_v}}_{\Phi_v} = 0 \quad (7)$$

for all  $q \in V$ . In practice, we consider a triangulation  $\mathcal{T}_h$  of the domain  $\Omega$  and we seek the solution in the finite element space  $\mathbb{P}_2(\mathcal{T}_h)$  of piecewise quadratic functions on  $\mathcal{T}_h$ .

### 2.2.2 Multiscale treatment of the vessel sources

The vessel, representing the source of oxygen, is assumed to be a thin tube, with radius much smaller than the characteristic length of the three-dimensional domain. Hence, in order to avoid an excessive mesh refinement close to the vessel, the boundary condition on  $\partial\Omega_v$  is treated in a multiscale fashion, adopting the *immersed boundary* formulation proposed in [7]. In this approach, the vessel is described only by a one-dimensional manifold  $\Gamma_v$ , representing the vessel axis (centerline), which does not need to be fully resolved by the finite element mesh, and it is *immersed* in the three-dimensional domain. Hence, it enters the diffusion equation (7) only as a singular flux term. In practice, the term  $\Phi_v$  in equation (7) is approximated by

$$\tilde{\Phi}_v = \left(\frac{1}{J_v}(c - c_v), q\right)_{\Gamma_v} \quad (8)$$

The main advantages of this approach is that it allows a coarser triangulation, as it does not need to fully resolve the vessel geometry, and at the same time, it can be easily adapted to arbitrary vessel configurations.

Using equation (8), the finite element formulation of equation (7) reads: Find  $c_h \in V_h$  such that

$$(D_{O_2} \nabla c_h, \nabla q_h)_\Omega + \sum_{\alpha=N,H,D} \mu_\alpha (R_\alpha^{cells}(t^{cells}) c_h, q_h)_\Omega + \left( \frac{1}{J_v} (c_h - c_v), q_h \right)_{\Gamma_v} = 0 \quad (9)$$

for all  $q_h \in V_{h,0}$ . Equation (9) is solved using a piecewise quadratic finite element method, implemented within the library FreeFem++ [16].

## 2.3 The coupled multiscale model

The multiscale model for glioblastoma is based on the coupled evolution of equation (3), the cell cycle and the oxygen diffusion (9).

In particular, the cellular tissue acts as a sink in the diffusion model (through the reaction terms  $R_N^{cells}$  and  $R_H^{cells}$ ), as cells might consume oxygen depending on their state. In turn, the concentration of oxygen influences the cell dynamics, as it is responsible of the variation of cell state (from normoxic to hypoxic and from hypoxic to dead).

The following sections describe in detail the coupling conditions, while Table 1 summarizes all the parameter used to define the coupled cell–oxygen model. Wherever possible the parameters were taken from the literature.

### 2.3.1 Coarsening of the cell distribution

The diffusion model is characterized by a coarser resolution than the cell model, as the variations of concentrations occur on a spatial scale larger than the cell typical size. As a result, the tetrahedral elements defining the computational mesh have a characteristic size much larger than the size of a cell. Hence, in order to obtain an efficient coupling scheme, the cell distributions  $R_{N,H}^{cells}$  have been *upscaled*, e.g. approximated by a piecewise constant functions defined according to the amount of cells in each tetrahedron at a given time.

### 2.3.2 Mapping of concentration field to cells

After computing the new stationary state for the oxygen concentration in the tissue (equation (9)), the value of oxygen for each cell is computed by evaluating

Table 1: Model parameters.

Parameter	Definition	Value [reference]
Cellular parameters		
$R_0$	Cell radius	5 – 10 $\mu\text{m}$
$T_{CC}$	Cell cycle	16 h
$\Delta t_{\text{cells}}$	Time step (cells)	1 min
$\alpha$	Adhesion coefficient	$3.1 \cdot 10^{-5} \text{ N/m}^2$ [26, 12]
$E$	Young modulus	1 kPa [26, 12]
$\nu$	Poisson ratio	0.5 [26]
$\gamma$	Cell-medium friction constant	24 $\mu\text{Nmin}/\mu\text{m}$
$D_c$	Random movement constant	$10^{-12} \text{ cm}^2/\text{s}$
$\tau_{\text{hypo}}^m$	Threshold (mean) normoxic $\rightarrow$ hypoxic	12 mmHg [21]
$\tau_{\text{hypo}}^v$	Threshold (variance) normoxic $\rightarrow$ hypoxic	5 mmHg
$\tau_{\text{dead}}$	Threshold hypoxic $\rightarrow$ dead	0.7 mmHg [21]
Oxygen parameters		
$D_{O_2}$	Diffusion constant	100 $\mu\text{m}^2/\text{s}$ [21]
$J_v$	Filtration coefficient	100 $\mu\text{m}^2$
$c_v$	Vessel concentration	60 mmHg [21]
$\mu_N$	Oxygen consumption rate per cell (normoxic)	$10^{-2}$ [21]
$\mu_H$	Oxygen consumption rate per cell (hypoxic)	$\frac{\mu_N}{5}$ [21]

the pointwise concentration field and its gradient at the cell center. Since the concentration is approximated as a piecewise quadratic finite element function, this is equivalent to a linear interpolation at the cell center, given the concentration field at the neighboring nodes of the finite element mesh.

### 3 Simulations results

We performed 3D simulations in a box-shaped domain of dimensions  $1800 \times 900 \times 900$  microns. An initial malignant cell is positioned at the centre of the domain as initial conditions. Moreover, two blood vessels are located at the left and right sides of the domain, from which oxygen is released into the environment (see Figure 4). Since the vessels are only represented by their centerline, and do not need to be explicitly resolved by the finite element mesh. Hence, the model can handle a wide range of vessel geometries. In particular, in order to avoid possible geometric artifacts, we chose an asymmetric configuration with the first vessel represented by a straight line in the vertical direction, and the second being a bifurcation.

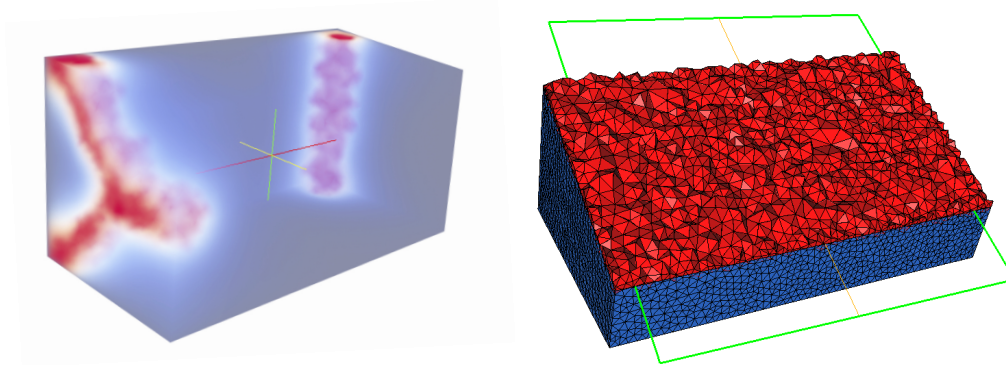


Figure 4: The domain used for the computational multi-scale simulations. Left: discrete representation of the blood vessels as immersed boundaries in the diffusion equation. In this approach, the vessels are not resolved within the mesh, but present in the equation as a singular term depending on the distance from the vessel centerline. Right: transversal cut of the finite element mesh used to solve the system.

### 3.1 Deterministic genotypes model

We first performed multi-scale simulations of a growing tumour using the deterministic genotypes model (DGM), where all the cells have equal genotype and respond identically under identical oxygen conditions. Figure 5 presents a view of the 3D simulation including oxygen dynamics. It can be observed how the oxygen concentration decreases concomitantly with the tumour grows. After about 14 days, an invasion process towards the vessels (colored in red in Figure 4, left) begins. A different view of the simulation results is displayed in Figure 6 (top,  $D = 0$ ). The cells are initially replicative (normoxic, blue cells) creating a multi-cellular spheroid. At certain moment the lack of oxygen determines a phenotypic change in those cells that do not have enough oxygen available. As a consequence, part of the tumour cells switch to anaerobic metabolism (hypoxic, white cells), activating migration mechanisms and starting an invasion process.

To determine the spatial zones of high cellular confluence Figure 7, top ( $D = 0$ ) shows a side view of the evolution of the cells experiencing a total repulsive force by the neighbours in contact over a determinate threshold  $\tau = 0.007\mu N$ .

It can be observed how, after 14 days, a palisade shape arises nearby the proliferative rim. The wave of invading cells is principally composed by normoxic (blue) and hypoxic (white) cells. This simulation satisfies the principal characteristics of a process of palisade formation: a set of cells migrate away from the tumour center forming a wall-like structure. However, the profile of the growing front may not be considered as an aggressive invasive tumour. Only a few cells succeed to escape

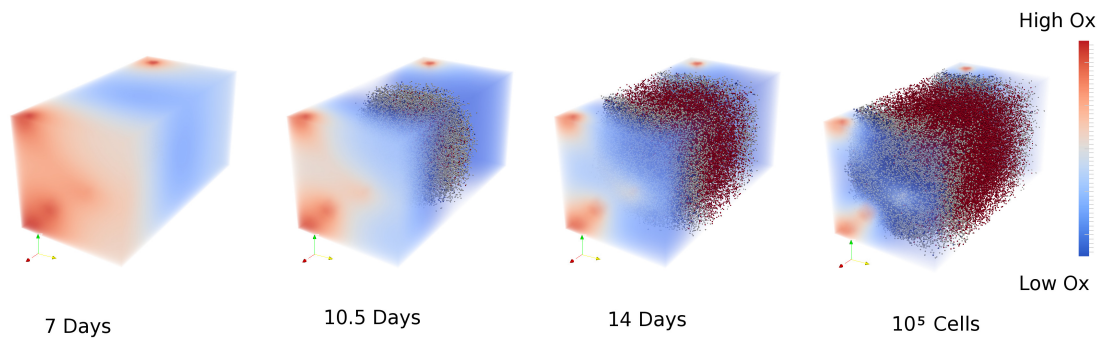


Figure 5: Temporal evolution of the tumour in the deterministic genotype model. Blue, white and red colours denote normoxic, hypoxic and death cells, while oxygen concentration is represented according the color bar on the right.

from the primary tumour and the outer rim of the tumour prevails homogenous and compact instead of disseminating within the nearby tissue.

### 3.2 Stochastic genotypes model

As next, to study the influence of a heterogeneous respond to oxygen concentrations of the malignant cells, we consider the stochastic genotype model (SGM), investigating the effect of increasing the value of the stochasticity ( $D$ ). Figure 6 shows the spatio-temporal evolution of 3 multi-scale simulations. The plot on the top corresponds to the DGM, i.e.  $D = 0$ , where every cell presents the same hypoxia threshold. It can be clearly observed that for the lower plots (for  $D = 10$  and  $D = 20$ , respectively) the invasive profile of the tumours is more aggressive. The outer rim is composed by a cloud of scattered cells that have colonized the neighborhood of the tumour. For intermediate stochasticity values ( $D = 10$ ) it can be observed how a similar phenotypic structure of layers as in the DGM arises. In contrast, further increasing the stochasticity ( $D = 20$ ), such stratified structure is not visible anymore.

Figure 7 shows the a comparison of the spatio-temporal evolution of the palisades (only the cells experiencing higher compressive values than  $\tau$ ). The simulation corresponding to the DGM (top figure,  $D = 0$ ) presents a well defined traveling front of malignant cells. This front is composed by a leading edge of replicative cells followed by a tail of hypoxic cells. This structure is closer to the traditional 3-layers multi-cellular spheroid than to a palisade. For intermediate levels of heterogeneity ( $D = 10$ ) the palisade presents a more invasive profile closer to the glioblastoma

clinical observations. The invasive front is composed by a cloud of scattered cells where the dominant phenotype is hypoxic. In addition, a relevant number of cells have succeeded to escape from the primary tumour.

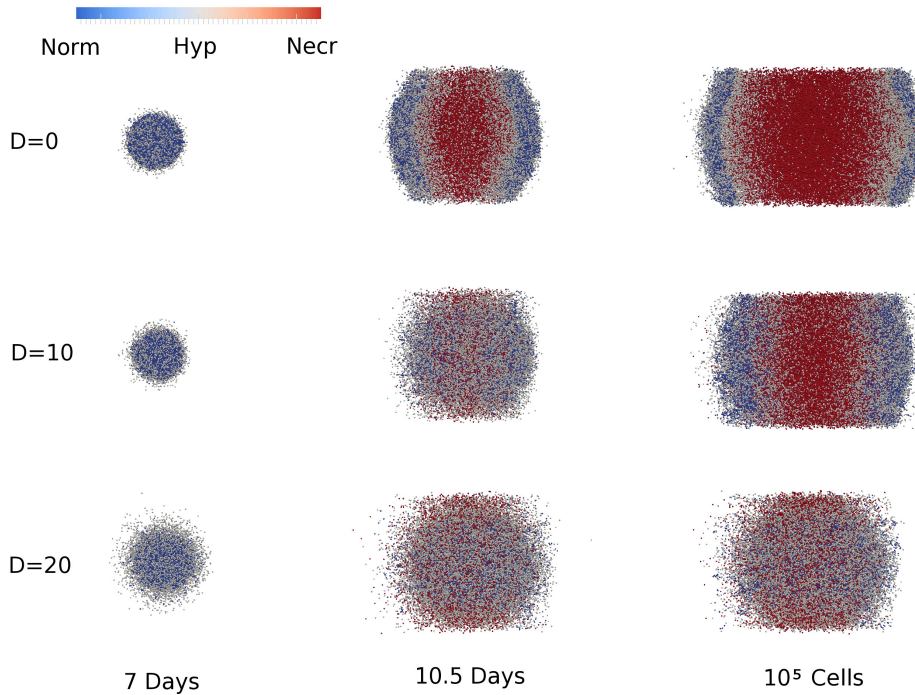


Figure 6: Temporal evolution of the tumour. Blue, white and red colours denote normoxic, hypoxic and death cells. The higher the stochasticity of the system is, the more invasive the tumours are.

The increase of stochasticity in the system allows the tumour to spread out through the nearby tissue loosing the compact profile of a non invasive tumour. The cells positioned at the proliferating rim are less affected by two important processes. Firstly, at the outer part, the competition for oxygen is less severe than in compact tumours due to lower cell confluence. This allows for the coexisting of a scattered population of normoxic and hypoxic cells at the invasive front. At the same time, lower cellular confluence hinders contact inhibition processes that have the potential of arresting cell cycle. And secondly, there exist a sub-population of cells that tolerate aerobic metabolism at lower oxygen levels. Thus the central part of the tumour presents also replicative cells.

### 3.2.1 Natural selection processes in the SGM

The plots in Figure 8 shows the spatio-temporal evolution of the cellular oxygen sensibility of the normoxic and hypoxic phenotypes for intermediate and high

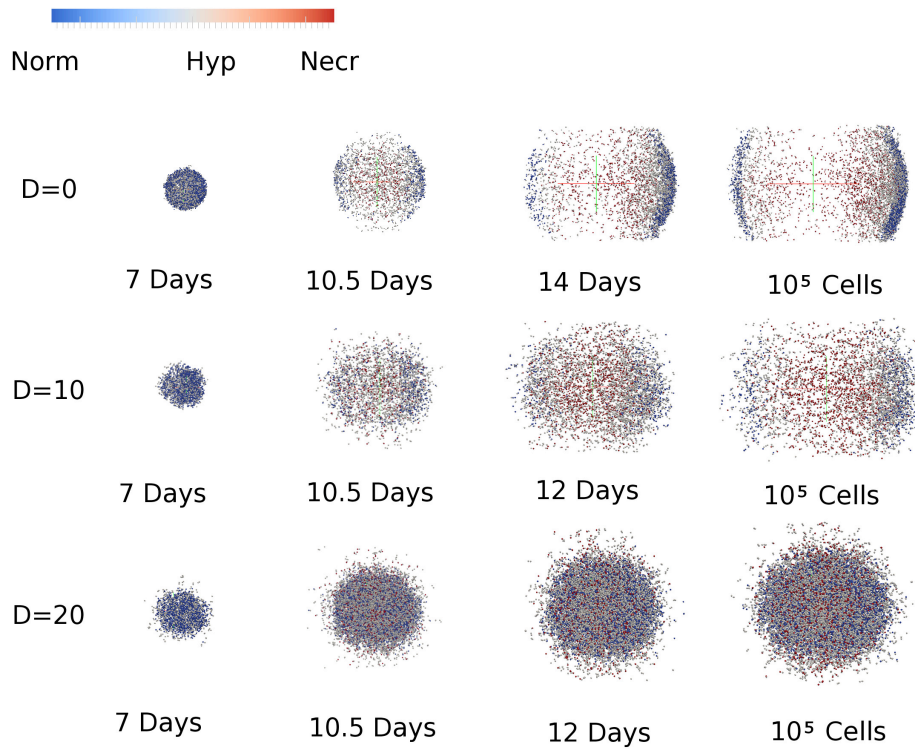


Figure 7: Temporal evolution of the areas of the tumour experiencing high cellular confluence (frontal view). As the tumour grows a palisade arises that invades the nearby tissue for the DGM and the intermediate stochasticity values of the SGM ( $D=10$ ). For high stochasticity values ( $D=20$ ) palisade formation cannot be observed.

stochasticity values ( $D=10$  and  $D=20$ ). The cells expressing lower oxygen threshold (dark blue) tend to be positioned at inner part of the tumour. In the model these cells are the ones that take longer to switch to anaerobic metabolism and enhance migration mechanism. In contrast, the cells expressing low oxygen thresholds (light blue to red) have succeeded to outcompete outer positions and some of them have scaped from the primary tumour. This result suggest that cells that are specially resistant to low oxygen conditions and activate migration mechanisms at low oxygen values are encapsulated at the central part of the tumour. At this position they risk dying of severe anoxia: the tumour mass may not allow cells to scape from the center for certain tumour sizes. Thus there exist a natural selection process: those cells that can perform aerobic metabolism at lower oxygen values have less probability to survive than those cells more sensitive to hypoxia that activate migration mechanisms earlier.

The left plot of Figure 9 shows the distribution of the transition thresholds (normoxic  $\rightarrow$  hypoxic) in three different tumours of about  $10^5$  cells of low ( $D=1$ ), inter-

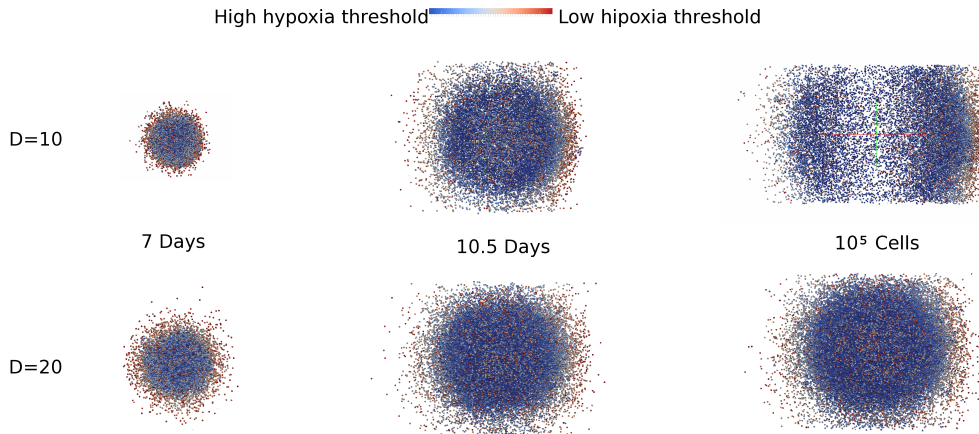


Figure 8: Tumour sections of two multi-scale simulations (only normoxic and hypoxic cells plotted) presenting different degrees of heterogeneity (variance  $\sigma = 5$  and variance  $\sigma = 10$ ). The colour of the cells denote the oxygen threshold at which cells change from normoxic to hypoxic phenotype and become invasive. Those cells that present a lower threshold (red) reach positions at the outer part of the tumours.

mediate ( $D = 5$ ) and high ( $D = 10$ ) stochasticity levels. It can be observed how there exists a selective process that yields a defined tendency for low oxygen threshold values. These are the cells that enhance sooner the migration mechanisms. The plot on the Figure 9 (right) shows the temporal evolution of the oxygen threshold values over a tumour of intermediate stochasticity ( $D = 5$ ). Moreover, it can be observed how the distribution changes over time abandoning the uniform initial shape to accumulate at low oxygen threshold values.

### 3.2.2 Tumor growth

Another direct consequence of the stochasticity concerns the the speed of growth. Figure 10 shows three different plots with the growing curves of normoxic, hypoxic and necrotic cell populations, for different stochasticity values. It can be observed that as the heterogeneity of the system increases, the tumours grows faster. This effect occurs in the three phenotypic sub-populations: normoxic, hypoxic and death, thus suggesting that heterogeneity in cell oxygen level sensibility is directly correlated to tumour growth [14].

In addition, the process of palisade formation seems to be delayed by oxygen sensibility heterogeneity. In the homogeneous ( $D = 0$ ) and in the low, and intermediate heterogeneity simulations ( $D = 2, 10$ ), the growth curves of the normoxic and hypoxic phenotypes show the transition to the stratified tumour structure (decrease

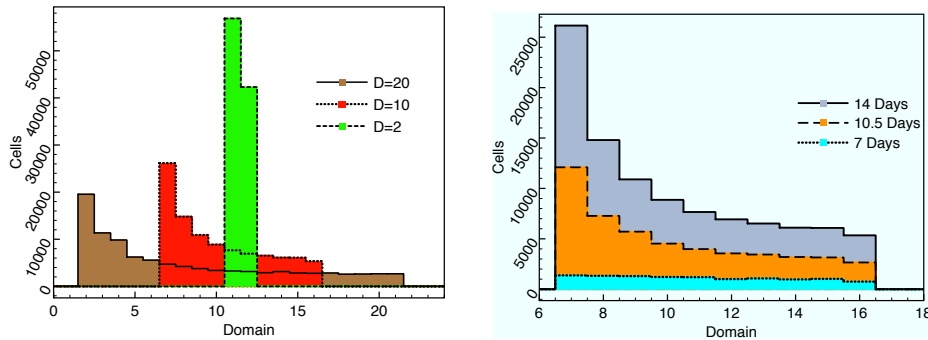


Figure 9: Evolutionary time dynamics of the heterogeneity of the genotypes. A clear tendency of natural selection towards cells that have low oxygen thresholds can be observed. Left: Distribution of oxygen thresholds for three different tumours of  $10^5$  cells. Right: Temporal evolution of the distribution of oxygen thresholds in a tumour of intermediate stochasticity values ( $D = 10$ ).

of normoxic and hypoxic growth curves speed) between days 7 and 10. This coincides with the arising of the palisade shape in Figure 7. For high heterogeneity values ( $D = 20$ ) this transition is not visible. However, the arise of a palisade can be predicted by the existing oscillations at the end of the growth plots of Figure 10 (normoxic and hypoxic, green line).

## 4 Conclusions and discussion

We presented a multiscale hybrid model (coupling an individual force-based for the cell population and and finite element method for the oxygen diffusion) for investigating the palisade formation and the relevance of genotypic heterogeneity. Our research allows to draw the following main conclusions:

- (1) The isolated structure of palisade formation can be explained by the traditional tumour stratified structure of necrotic-hypoxic-replicative layers. However, these conditions are not sufficient to explain the invasion of the local environment by malignant cells. Local invasion can arise by the heterogeneity produced in a cellular population caused by variations in the hypoxia switch, or by similar mechanisms [20] that may produce a highly heterogeneous population. Cancer cell heterogeneity is known to be a constant in malignant tumour of different types of cancers and can be exploited as a research field to improve treatments.
- (2) The degree of heterogeneity within the tumour cellular population is directly correlated with tumour growth speed. Both biological experiments and theoretical models have shown for different protein pathways that heterogeneity enhances tu-

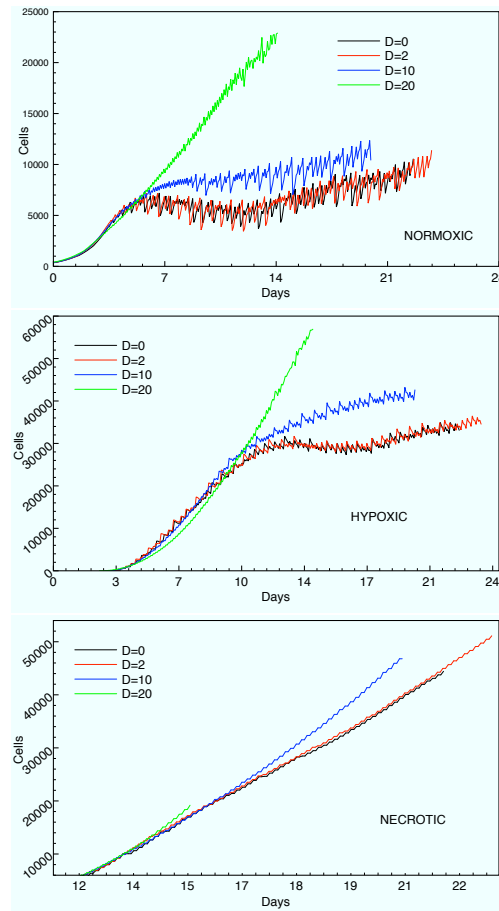


Figure 10: Growth curves for different variance values of the normoxic, hypoxic and necrotic phenotypes. The increase of variance enhances tumour growth speed.

mour invasiveness. According to the aerobic-anaerobic metabolism we have shown that heterogeneity does not only promotes invasion but also enhances cellular proliferation (this finding is in agreement with [14]). In our simulations, this result is probably due to a combination of cell migration and cellular contact inhibition processes. When cells of similar characteristics compete against each other, the tumour grows as an unified compact mass of cells. In contrast, when the phenotypic response is heterogenous, those cells that succeed to gain distant positions relief the tumour cell density and, as a result, the contact inhibition process is deactivated.

(3) Hypoxia conditions generate a Darwinian competition scenario where the most hypoxia-resistant cells remain at the central part of the tumour, while those cells that switch earlier to anaerobic metabolism outcompete to gain distant locations. Experimental results have shown in multi-cellular spheroids that the cells at the in-

ner part behave differently than those cells at the outer rim. Our model suggest that competition processes determine a selective gradient where those cells that activate later the migrating mechanisms remain at the centre of the tumour. Activation of the cellular migration machinery is directly correlated with the switch to anaerobic metabolism via HIF-1 $\alpha$  [21, 24, 22]. Therefore, according to our results, we hypothesize that those cells that activate HIF-1  $\alpha$  at lower levels of oxygen remain at the central part of the tumour. This suggests that the non-necrotic inner part of the tumour may function as a pool of highly resistant cells to anaerobic conditions, having the potential for creating stronger recursive tumours after chemotherapy treatment.

## References

- [1] M. E. Berens and A. Giese, *Those left behind. Ó Biology and Oncology of Invasive Glioma Cells*, Neoplasia **1** (1999), no. 3, 208–219.
- [2] Daniel J. Brat, Amilcar A. Castellano-Sanchez, Stephen B. Hunter, Marcia Pecot, Cynthia Cohen, Elizabeth H. Hammond, Sarojini N. Devi, Balveen Kaur, and Erwin G. Van Meir, *Pseudopalisades in glioblastoma are hypoxic, express extracellular matrix proteases, and are formed by an actively migrating cell population*, Cancer Research **64** (2004), no. 3, 920–927.
- [3] Daniel J. Brat and Erwin G. Van Meir, *Vaso-occlusive and prothrombotic mechanisms associated with tumor hypoxia, necrosis, and accelerated growth in glioblastoma*, Lab Invest **84** (2004), no. 4, 397Ð405.
- [4] A. Caiazzo, D. Evans, J.-L. Falcone, J. Hegewald, E. Lorenz, B. Stahl, D. Wang, J. Bernsdorf, B. Chopard, J. Gunn, R. Hose, M. Krafczyk, P. Lawford, R. Smallwood, D. Walker, and Hoekstra A.G., *A complex automata approach for in-stent restenosis: two-dimensional multiscale modeling and simulations*, J. Comp. Sc. **2** (2011), no. 1, 9–17.
- [5] C. Carmona-Fontaine, V. Bucci, L. Akkari, M. Deforet, J. A. Joyce, and J. B. Xavier, *Emergence of spatial structure in the tumor microenvironment due to the Warburg effect*, Proceedings of the National Academy of Sciences (2013), 19402–19407.
- [6] Paul J. Choi, Long Cai, Kirsten Frieda, and X. Sunney Xie, *A stochastic single-molecule event triggers phenotype switching of a bacterial cell*, Science **322** (2008), no. 5900, 442–446.
- [7] C. D’Angelo and A. Quarteroni, *On the Coupling of 1D and 3D Diffusion-Reaction Equations. Application to Tissue Perfusion Problems*, M3AS **18** (2008), no. 8, 1481–1504.

- [8] A. Daçu, I. Toma-Daçu, and M. Karlsson, *Theoretical simulation of tumour oxygenation and results from acute and chronic hypoxia*, *Physics in Medicine and Biology* **48** (2003), no. 17, 2829.
- [9] H. Enderling, L. Hlatky, and P. Hahnfeldt, *Migration rules: tumours are conglomerates of self-metastases*, *Br J Cancer* **100** (2009), no. 12, 1917–1925.
- [10] S. Fujiwara, K. Nakagawa, H. Harada, S. Nagato, K. Furukawa, M. Teraoka, T. Seno, K. Oka, S. Iwata, and T. Ohnishi, *Silencing hypoxia-inducible factor-1 $\alpha$  inhibits cell migration and invasion under hypoxic environment in malignant gliomas*, *International Journal of Oncology* **30** (2007), no. 4, 793–802.
- [11] F. B. Furnari, T. Fenton, R. M. Bachoo, A. Mukasa, J. M. Stommel, A. Stegh, W. H. Keith, L. Ligon, D. N. Louis, C. Brennan, L. Chin, R. A. DePinho, and W. K. Cavenee, *Malignant astrocytic glioma: genetics, biology, and paths to treatment*, *Genes and Development* **28** (2007), 2683–2710.
- [12] J. Galle and D. Drasdo, *Modeling the effect of deregulated proliferation and apoptosis on the growth dynamics of epithelial cell populations in vitro*, *Biophysical Journal* **88** (2009), 62–75.
- [13] R. A. Gatenby, *Why do cancers have high aerobic glycolysis?*, *Nat. Rev. Canc.* **4** (2004), no. 11, 891–899.
- [14] P. Gerlee and S. Nelander, *The impact of phenotypic switching on glioblastoma growth and invasion*, *PLoS Comput Biol* **8** (2012), no. 6, e1002556.
- [15] P. B. Gupta, C. M. Fillmore, G. Jiang, S. D. Shapira, K. Tao, C. Kuperwasser, and E. S. Lander, *Stochastic State Transitions Give Rise to Phenotypic Equilibrium in Populations of Cancer Cells*, *Cell* **146** (2014), no. 4, 633–644.
- [16] F. Hecht, *Freefem++ v. 3.13. user's manual*, University of Paris 6, 2014.
- [17] A.G. Hoekstra, E. Lorenz, J.L. Falcone, and B. Chopard, *Towards a complex automata framework for multi-scale modeling: Formalism and the scale separation map*, *Proceedings of 7th ICCS, LNCS 4487*, Springer-Verlag, Berlin, Heidelberg, 2007, pp. 922–930.
- [18] L. Holmquist, A. Jögi, and S. Pahlman, *Phenotypic persistence after reoxygenation of hypoxic neuroblastoma cells*, *International Journal of Cancer* **116** (2005), no. 2, 218–225.
- [19] W. Johannsen, *The genotype conception of heredity*, *The American Naturalist* **45** (1911), no. 531, pp. 129–159.

- [20] M. Kim, D. Reed, and K. A. Rejniak, *The formation of tight tumor clusters affects the efficacy of cell cycle inhibitors: A hybrid model study*, Journal of Theoretical Biology **352** (2014), no. 0, 31 – 50.
- [21] A. Martínez-González, G. F. Calvo, L. A. Pérez-Romasanta, and V. M. Pérez-García, *Hypoxic cell waves around necrotic cores in glioblastoma: A biomathematical model and its therapeutic implications*, Bulletin of Mathematical Biology **74** (2012), no. 12, 2875–2896.
- [22] A. Martínez-González, M. Durán-Prado, G. F. Calvo, F. J. Alcaín, L. A. Pérez-Romasanta, and V. M. Pérez-García, *Combined therapies of antithrombotics and antioxidants delay in silico brain tumour progression*, Mathematical Medicine and Biology (in press) (2014).
- [23] V. Matyash and H. Kettenmann, *Heterogeneity in astrocyte morphology and physiology*, Brain Research Reviews **63** (2010), no. 1–2, 2–10.
- [24] R. Pardo, A. Martínez-Gonzalez, and V. M. Pérez-García, *Waves of cells with an unstable phenotype accelerate the progression of high-grade brain tumors*, arXiv:1405.0369 [q-bio.QM] (2014).
- [25] I. Ramis-Conde, M. A. J. Chaplain, A. R. A. Anderson, and D. Drasdo, *Multi-scale modelling of cancer cell intravasation: the role of cadherins in metastasis*, Physical Biology **6** (2009), no. 1, 016008.
- [26] I. Ramis-Conde and D. Drasdo, *From genotypes to phenotypes: classification of the tumour profiles for different variants of the cadherin adhesion pathway*, Physical Biology **9** (2012), no. 3, 036008.
- [27] I. Ramis-Conde, D. Drasdo, A. R. A. Anderson, and M. A. J. Chaplain, *Modeling the influence of the e-cadherin- $\beta$ -catenin pathway in cancer cell invasion*, Biophysical Journal **95** (2008), no. 1, 155–165.
- [28] D. S. Rickman, M. P. Bobek, D. E. Misek, R. Kuick, M. Blaivas, D. M. Kurnit, J. Taylor, and S. M. Hanash, *Distinctive molecular profiles of high-grade and low-grade gliomas based on oligonucleotide microarray analysis*, Cancer Research **61** (2001), no. 18, 6885–6891.
- [29] M. R. Robinson, N. R. Wray, and P. M. Visscher, *Explaining additional genetic variation in complex traits*, Trends in Genetics **30** (2014), no. 4, 124 – 132.
- [30] D. Schlueter, I. Ramis-Conde, and M. A. J. Chaplain, *Computational modeling of single-cell migration: The leading role of extracellular matrix fibers*, Biophysical Journal **103** (2012), no. 6, 1141 – 1151.
- [31] P.M.A. Slood and A.G. Hoekstra, *Multiscale modeling in computational biology*, Briefings in Bioinformatics **11** (2010), 142–152.

- [32] A. Sottoriva, I. Spiteri, S. G. M. Piccirillo, A. Touloumis, V. P. Collins, J. C. Marioni, C. Curtis, C. Watts, and S. Tavaré, *Intratumor heterogeneity in human glioblastoma reflects cancer evolutionary dynamics*, Proceedings of the National Academy of Sciences **110** (2013), no. 10, 4009–4014.
- [33] Y. Taniguchi, P. J. Choi, G.-W. Li, Huiyi Chen, M. Babu, J. Hearn, A. Emili, and X. S. Xie, *Quantifying e. coli proteome and transcriptome with single-molecule sensitivity in single cells*, Science **329** (2010), no. 5991, 533–538.
- [34] P. Thomas, P. Nikola, and R. Grima, *Phenotypic switching in gene regulatory networks*, Proceedings of the National Academy of Sciences **111** (2014), no. 19, 6994–6999.
- [35] P. Tracqui, G. C. Cruywagen, D. E. Woodward, G. T. Bartoo, J. D. Murray, and E. C. Alvord, *A mathematical model of glioma growth: the effect of chemotherapy on spatio-temporal growth*, Cell Proliferation **28** (1995), no. 1, 17–31.